Acetylcholine ameliorates colitis by promoting IL-10 secretion of monocytic myeloid-derived suppressor cells through the nAChR/ERK pathway

Wanwei Zheng[a,1], Huan Song[a,b,1], Zhongguang Luo[a,1], Hao Wu[c,1], Lin Chen[a], Yuedi Wang[b,d], Haoshu Cui[a], Yufei Zhang[e], Bangting Wang[a], Wenshuai Li[a], Yao Liu[a], Jun Zhang[a], Yiwei Chu[b,d,f,2], Feifei Luo[a,b,2], and Jie Liu[a,b,d,f,g,2]

[a]Department of Digestive Diseases, Huashan Hospital, Fudan University, Shanghai 200040, China; [b]Biotherapy Research Center of Fudan University and Shanghai Engineering Technology Research Center of Intelligent Cancer Medicine, Shanghai 200032, China; [c]Department of Dermatology, Huashan Hospital, Fudan University, Shanghai 200040, China; [d]Department of Immunology, School of Basic Medical Sciences, Fudan University, Shanghai 200032, China; [e]Fosun Lead (Shanghai) Healthcare Technologies Co., Ltd., Shanghai 200437, China; [f]Institutes of Biomedical Sciences and State Key Laboratory of Genetic Engineering, Fudan University, Shanghai 200032, China and [g]Shanghai Key Laboratory of Metabolic Remodeling and Health, Institute of Metabolism & Integrative Biology, Fudan University, Shanghai 200433, China

Edited by Lawrence Steinman, Stanford University School of Medicine, Stanford, CA, and approved February 1, 2021 (received for review August 22, 2020)

The alteration of the enteric nervous system (ENS) and its role in neuroimmune modulation remain obscure in the pathogenesis of inflammatory bowel diseases (IBDs). Here, by using the xCell tool and the latest immunolabeling-enabled three-dimensional (3D) imaging of solvent-cleared organs technique, we found severe pathological damage of the entire ENS and decreased expression of choline acetyltransferase (ChAT) in IBD patients. As a result, acetylcholine (ACh), a major neurotransmitter of the nervous system synthesized by ChAT, was greatly reduced in colon tissues of both IBD patients and colitis mice. Importantly, administration of ACh via enema remarkably ameliorated colitis, which was proved to be directly dependent on monocytic myeloid-derived suppressor cells (M-MDSCs). Furthermore, ACh was demonstrated to promote interleukin-10 secretion of M-MDSCs and suppress the inflammation through activating the nAChR/ERK pathway. The present data reveal that the cholinergic signaling pathway in the ENS is impaired during colitis and uncover an ACh-MDSCs neuroimmune regulatory pathway, which may offer promising therapeutic strategies for IBDs.

ACh | M-MDSCs | IL-10 | nAChR/ERK | IBD

The enteric nervous system (ENS), consisting of neurons and glial cells, spans the length of gastrointestinal (GI) tract, especially in two distinct layers of interconnected ganglia, the outer myenteric and the inner submucosal plexus (1–4). The ENS has been found to control virtually all aspects of physiology of the GI tract, including motility, secretion, absorption, and local immunity (1–3, 5). Evidence is accumulating that the bidirectional interaction between the ENS and the intestinal immune system operates as a critical hub for the maintenance of intestinal homeostasis (5, 6).

Inflammatory bowel diseases (IBDs) are a group of disorders that involve chronic inflammation of the GI tract, which are characterized by immune-mediated destruction of intestinal homeostasis (7). Several studies have displayed that the ENS was altered in an IBD mice model and in patients (8–11). However, there is no consistent knowledge about how the ENS is altered during IBD or whether the alteration of the ENS contributes to the severity of intestinal inflammation. It is reported that the loss of neurons that happened in IBDs led to disruption of colonic motor activity (8, 10). In contrast, the locally increased density of neurons contributed to intestinal inflammation (11). The underlying mechanisms that mediate the connection between the ENS and intestinal inflammation are poorly understood.

It is known to all that neurotransmitters are the main executors in the nervous system. Acetylcholine (ACh), as a primary neurotransmitter in both the central and peripheral nervous systems, is produced by choline acetyltransferase (ChAT). Two types of ACh receptors have been identified on immune cells, muscarinic and nicotinic ACh receptors (mAChRs and nAChRs, respectively), both of which are involved in manipulation of immune cell function by modulating cholinergic activity (5, 12). For example, activation of nAChRs such as α7 nAChR on immune cells attenuated the synthesis and release of proinflammatory cytokine tumor necrosis factor (TNF)-α in lipopolysaccharide (LPS)-activated macrophages (13). The deficiency of mAChRs (both type1 and type5) significantly diminished TNF-α, interferon (IFN)-γ, and interleukin (IL)-6 secretions of splenocytes upon ovalbumin stimulation (14). Thus, the ACh-mediated cholinergic pathway may participate in mitigating exuberant inflammation in intestine, which has not been fully elucidated.

Myeloid-derived suppressor cells (MDSCs) are a heterogeneous population of myeloid-derived cells composed of monocytes and neutrophils arrested in an immature state, which

Significance

Inflammatory bowel diseases (IBDs) have been characterized by immune-mediated destruction of intestinal homeostasis. Until now, there have been no optimal therapies due to lack of a comprehensive understanding on pathophysiology during IBDs. The enteric nervous system (ENS) is emerging as a critical participant in intestinal immunomodulation, but the interaction between the ENS and intestinal immunity in IBDs remains unclear. Here, we discover the alteration of the ENS featured with reduced neurons and decreased acetylcholine (ACh) in IBDs. Moreover, ACh directly enhances the antiinflammatory activity of monocytic myeloid-derived suppressor cells by promoting interleukin-10 production through nicotinic ACh receptors, and thus ameliorates colitis. Our data highlight a neuroimmunomodulatory pathway and provide an alternative avenue by locally increasing ACh level for IBD therapy.

Author contributions: Z.L., F.L., and J.L. designed research; W.Z., H.S., L.C., Y.W., H.C., Y.Z., B.W., W.L., Y.L., J.Z., and F.L. performed research; W.Z., H.S., and F.L. analyzed data; and W.Z., H.S., Z.L., H.W., Y.C., F.L., and J.L. wrote the paper.

The authors declare no competing interest.

This article is a PNAS Direct Submission.

[1]W.Z., H.S., Z.L., and H.W. contributed equally to this work.

[2]To whom correspondence may be addressed. Email: yiweichu@fudan.edu.cn, feifeiluo@fudan.edu.cn, or jieliu@fudan.edu.cn.

This article contains supporting information online at https://www.pnas.org/lookup/suppl/doi:10.1073/pnas.2017762118/-/DCSupplemental.

Published March 8, 2021.

migrate from the bone marrow to the periphery and to the site of inflammation, and mediate immunosuppression (15–18). Two subsets of MDSCs have been defined, $CD11b^{+}Ly6G^{-}Ly6C^{high}$ monocyte-like MDSCs (monocytic MDSCs, M-MDSCs) and $CD11b^{+}Ly6G^{+}Ly6C^{low}$ granulocyte-like MDSCs (granulocytic MDSCs, G-MDSCs) (19–23). Compared with G-MDSCs, M-MDSCs exhibit a higher suppressive capacity mainly by producing nitric oxide, transforming growth factor (TGF)-β and IL-10 (18, 22, 23). Previous studies have discovered an obvious accumulation of MDSCs in the colon of IBD patients and colitis mice (21, 22, 24). Furthermore, infusion of MDSCs could effectively suppress effector T cell-mediated inflammatory response and prevent the occurrence of lethal inflammation, while the blockade of MDSCs would significantly increase the mortality rate of colitis mice (20, 25–28). Hence, MDSCs have been considered as a candidate for IBD therapy. In view of AChR expression on myeloid cells, to deeply understand the relationship between MDSCs and the ACh-mediated cholinergic pathway might help explore new therapeutic strategies for IBD, which have not been investigated yet.

Herein, we first performed a computational cell-type enrichment analysis (xCell), and an immunolabeling-enabled three-dimensional (3D) imaging of solvent-cleared organs technique (iDISCO), to evaluate the alteration of the ENS in IBDs. Our data suggested that the enteric neuronal network was disrupted in ulcerative colitis (UC) patients and colitis mice, accompanied by down-regulated expression of ChAT and reduced production of ACh. Moreover, administration of ACh remarkably ameliorated intestinal inflammation via activating the nAChR/ERK/IL-10 pathway in M-MDSCs. These results uncover a neuroimmune regulatory mechanism and may provide potential strategies for IBD treatment.

Results

Reduced Density of Neurons Is Positively Correlated with ChAT Expression, Resulting in Impaired ACh Production. The ENS is widely distributed in various layers of the intestine (1–3). Due to the limited use of imaging techniques, it is still full of conflicts and controversies as to whether and how the ENS is altered in IBDs. In order to comprehensively display the portrait of the ENS during colitis, the xCell webtool (29) and the iDISCO method (30) were utilized. According to the results of xCell analyzed from a Gene Expression Omnibus (GEO) dataset, xCell enrichment scores (estimated proportion of cell types calculated for each sample) of neurons in the colon of UC patients at the active stage (A-UC) were remarkably lower than those in healthy controls and UC patients of the remission stage (R-UC) (Fig. 1*A*). Meanwhile, Pearson's correlation coefficients between the xCell scores of neurons and the mRNA levels of neurotransmitter metabolism-related genes were displayed by heatmap (Fig. 1*B*). Notably, ChAT was the most positively correlated gene with neuron xCell scores (Fig. 1 *B* and *C*). To confirm the above phenomenon, colon samples collected from healthy donors or UC patients at the active stage were cleared by solvent, stained with neurofilament medium/heavy polypeptide (NF-M/H), and detected by two-photon imaging. The 3D imaging proved that density of neurons was reduced and neuronal network structure was dramatically disrupted in the submucosal plexus of UC patients when compared with those in healthy donors (Fig. 1*D*). In addition, dual-labeled immunohistochemistry showed that the density of $ChAT^{+}$ neurons in submucosal plexus was markedly decreased in UC patients (Fig. 1*E*). Then, to further address whether the reduced $ChAT^{+}$ neurons in submucosal plexus would impair the production of ACh, ultra high pressure liquid chromatography coupled to tandem mass spectrometry (UHPLC-MS/MS) was used to determine the level of ACh in the colon. In agreement with the aforementioned results, the level of ACh was significantly lower in UC patients than that in healthy controls (Fig. 1*F*). Therefore, these results indicate that severe ENS damage occurs in IBD patients, which is accompanied by reduced ChAT expression and decreased ACh production in the colon.

ACh Significantly Alleviates Ongoing Colitis in a Mice Model. To investigate the alternation of the ENS in colitis mice, we established a dextran sulfate sodium (DSS)-induced colitis model, which has been widely used due to the similar clinical, immunological, and histological features of UC in humans (31). Consistent with the above observations in UC patients, the density of neurons (Fig. 2*A*) and mRNA expression of *Chat* (Fig. 2*B*) were significantly reduced in colons of colitis mice compared with control mice. As a result, the production of colonic ACh in colitis mice was remarkably down-regulated when compared with that in control mice (Fig. 2*C*). To further determine the role of ACh on colitis, C57BL/6 mice were fed water containing 3% DSS for 7 d, and these mice received ACh via enema every other day for a total of three times, starting from the second day. Intriguingly, administration of ACh significantly attenuated DSS-induced weight loss (Fig. 2*D*), disease activity index (DAI) increase (Fig. 2*E*), and colon length shortening (Fig. 2*F*) of mice. Detailed histological analysis of colonic lesions showed that ACh treatment markedly mitigated pathological changes, including mucosal architecture disruption, inflammatory cell infiltration, and foci of crypt loss, which led to lower histological scores (Fig. 2*G*). Furthermore, the mRNA expression of intestinal proinflammatory cytokines, TNF-α, IFN-γ, IL-17A, IL-1β, and IL-6, was greatly down-regulated in response to ACh treatment, while the antiinflammatory cytokine IL-10 was remarkably up-regulated (Fig. 2*H*). Additionally, the enzyme-linked immunosorbent assay (ELISA) validated the above changes of anti- or proinflammatory cytokines in the protein level (Fig. 2*I*). Taken together, these data strongly suggest that administration of ACh via enema alleviates ongoing intestinal inflammation and provides therapeutic benefits for colitis mice.

M-MDSCs Are Critical for ACh-Mediated Resistance against Colitis. To explore how ACh ameliorates experimental colitis, we first set up a primary colonic organoid culture system to study the impact of ACh on intestinal epithelial cells (IECs). After treatment of H_2O or ACh for 72 h, no difference could be found in the size of the colonic organoids (*SI Appendix*, Fig. S1*A*). The mRNA levels of proliferation-related genes, *Lgr5*, *Olfm4*, and *Ascl2*, were similar between ACh-treated colonic organoids and H_2O-treated ones (*SI Appendix*, Fig. S1*B*). These results exclude the direct impact of ACh on the proliferation of IECs.

Next, considering the critical role of immune system in the pathogenesis of IBDs, we analyzed the immune cell subpopulations in the blood, spleen, and colon derived from H_2O- or ACh-treated colitis mice by flow cytometry. The gating strategy for myeloid cells is shown in Fig. 3*A*. Interestingly, a significant increase was found merely in the frequency of M-MDSCs in colonic lamina propria (cLP) of ACh-treated colitis mice, but not macrophages, dendritic cells, eosinophils, or G-MDSCs (Fig. 3*B*), which have been reported to be involved in colitis (32, 33). Meanwhile, the frequency of T helper (Th) 17 cells in cLP was greatly decreased after ACh treatment (*SI Appendix*, Fig. S2*A*). There were no obvious differences in the frequencies of both myeloid cells and T cell subsets derived from blood and spleens between H_2O- and ACh-treated colitis mice (*SI Appendix*, Fig. S2 *B* and *C*), indicating that ACh only influenced local immunity but not systemic immunity. Previous studies have reported that Th cells play proinflammatory or antiinflammatory roles in DSS-induced colitis (34, 35). The reduced frequency of colon-infiltrating Th17 cells was observed after ACh treatment. Hence, the impact of ACh on Th cell proliferation, differentiation, and function, especially Th17 cells, need to be addressed.

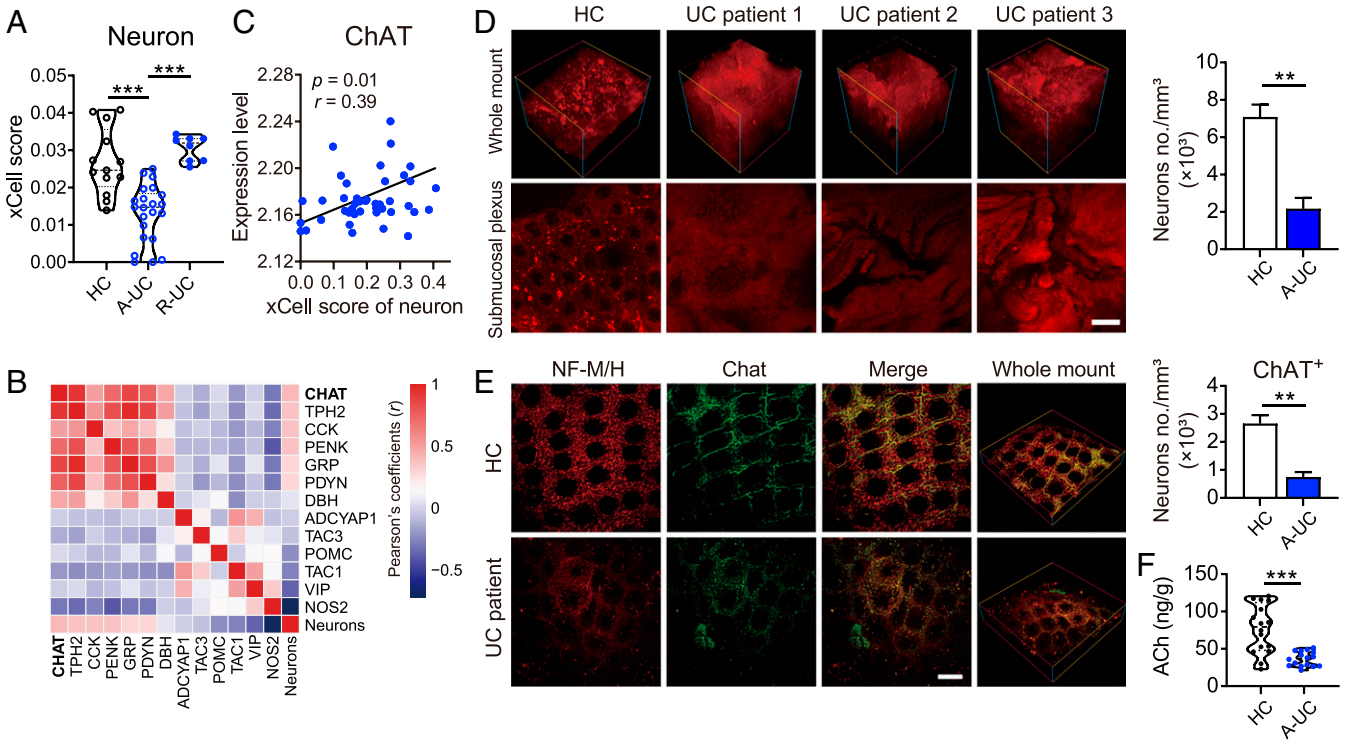

Fig. 1. The impaired neuronal network is accompanied by reduced ChAT expression and ACh production in UC patients. (*A*) Neuron proportions in the colon of healthy controls (HC, $n = 13$) and ulcerative colitis patients in remission (R-UC, $n = 8$) or active (A-UC, $n = 22$) stage were calculated using xCell. (*B* and *C*) Correlation analysis between percentage of neuron and expression of genes involved in neurotransmitter synthesis and metabolism. Pearson's correlation coefficients (r) are indicated for each correlation in *B* and *C* and *P* values are indicated in *C*. Red, positive correlation; blue, negative correlation ($n = 43$). (*D*) Representative multiphoton fluorescence imaging showed neuronal network of submucosal plexus in IBD patients. Neurons were labeled for NF-M/H (red). (Scale bar, 100 μm.) The number of neurons was determined by ImageJ and normalized to total sample volume ($n = 4$). (*E*) Representative colon tissues of UC patients and healthy controls stained for NF-M/H (red) and ChAT (green). (Scale bar, 100 μm.) The number of neurons was determined by ImageJ and normalized to total sample volume ($n = 4$). (*F*) The level of ACh in colon of UC patients and HCs was measured using UPLC-MS/MS ($n = 17$). Data are expressed as mean ± SEM. Statistical differences were tested using one-way ANOVA in *A* followed by post hoc Bonferroni's test, and unpaired two-tailed Student's *t* test in *D*–*F*. $^{**}P < 0.01$, and $^{***}P < 0.001$.

$CD4^+$ T cells were isolated from colitis mice and stimulated with different doses of ACh (*SI Appendix*, Fig. S3*A*). However, comparable frequencies of Th cells were found among ACh treatment groups and control groups. Furthermore, purified naïve $CD4^+$ T cells were treated with TGF-β and IL-6 to generate Th17 cells, with or without ACh stimulation for 3 d. The frequency of Th17 cells and the production of IL-17A in the ACh-stimulated group were both similar with those in the control group (*SI Appendix*, Fig. S3 *B* and *C*). These findings suggest that Th17 cells are not directly responsive to ACh stimulation in vitro.

MDSCs are divided into M-MDSCs ($CD11b^+Ly6G^-Ly6C^{hi}$) and G-MDSCs ($CD11b^+Ly6G^+Ly6C^{lo}$) based on their different morphologies and immunophenotypes (21, 23). M-MDSCs have been recognized as more strongly negative regulators than G-MDSCs in many pathological conditions (18, 23). But numerous studies concerning colitis defined MDSCs as $CD11b^+Gr\text{-}1^+$ ($Ly6G^+Ly6C^+$) without further classification, which probably limit the understanding of the biology and clinical application of these cells in IBDs. Since ACh treatment only led to the significant increase of M-MDSCs but not G-MDSCs in cLP in our in vivo experiment, we purified colonic M-MDSCs and G-MDSCs from colitis mice for RNA sequencing analysis (RNA-seq). The RNA-seq results displayed that the gene expression profiles of G-MDSCs and M-MDSCs were markedly distinct (*SI Appendix*, Fig. S4 *A* and *B*). Meanwhile, splenocytes derived from colitis mice were stimulated with different doses of ACh for 24 h. Only the frequency of M-MDSCs but not G-MDSCs was elevated remarkably in response to ACh stimulation, especially at the dose of 100 μM, which would be used in the following ACh in vitro stimulation experiments (*SI Appendix*, Fig. S5*A*). Furthermore, G-MDSCs isolated from cLP were treated with ACh or H_2O for RNA-seq. However, representative surface and function markers of G-MDSCs were unaffected after ACh stimulation for 16 h (*SI Appendix*, Fig. S5*B*). These in vivo and in vitro data suggest that ACh selectively boosts M-MDSCs, and thus M-MDSCs may play a role in the ACh-mediated suppression of intestinal inflammation.

In order to confirm the above speculation, we depleted M-MDSCs by intraperitoneally injecting anti-Gr-1 monoclonal antibody (αGr-1) in the colitis model. Consistent with previous studies, αGr-1 antibody effectively depleted MDSCs (both M-MDSCs and G-MDSCs) in the peripheral blood and cLP (*SI Appendix*, Fig. S6). Notably, the beneficial effects of ACh on classical signs of colitis including weight loss (Fig. 3*C*), DAI (Fig. 3*D*), colon length shortening (Fig. 3*E*), and colonic histological score (Fig. 3*F*), were impaired greatly upon αGr-1 antibody administration. Collectively, our results demonstrate that M-MDSCs are required for ACh-mediated protection against ongoing intestinal inflammation.

ACh Enhances the Antiinflammatory Effects of M-MDSCs by Increasing IL-10 Production. To carefully investigate the effect of ACh treatment on M-MDSCs, M-MDSCs were sorted by flow cytometry and stimulated with ACh for 24 h. It was observed that ACh stimulation didn't alter the expression of the proliferative marker Ki67 (*SI Appendix*, Fig. S7*A*), but promoted the survival

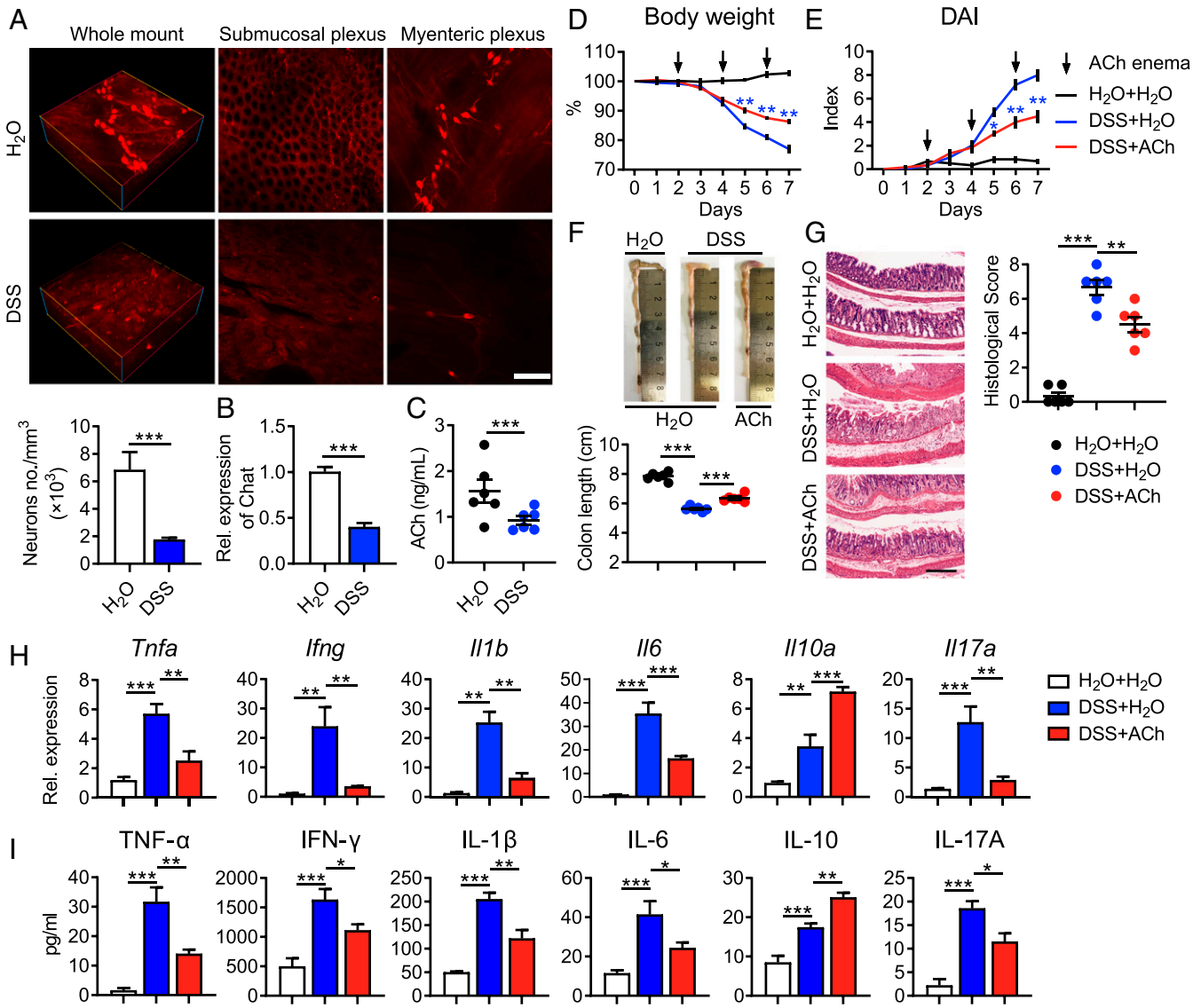

Fig. 2. Administration of ACh alleviates ongoing colitis. Female C57BL/6 mice receiving water containing 3% DSS (wt/vol) or regular drinking water alone for 7 d, were treated with 50 μL H_2O or 25 mg/kg ACh in 50 μL H_2O via enema every other day for a total of three times, starting from day 2. (*A*) Representative multiphoton fluorescence imaging showed the whole-mount, submucosal plexus and myenteric plexus from wild-type (WT, H_2O) or colitis mice (DSS). Neurons were labeled for NF-M/H. (Scale bar, 100 μm.) The number of neurons was determined by ImageJ and normalized to total sample volume ($n = 4$). (*B*) *Chat* expression of colon tissues from WT or colitis mice was detected by quantitative RT-PCR ($n = 4$). (*C*) The level of ACh in colon tissues of WT or colitis mice was detected using UPLC-MS/MS ($n = 6$). (*D* and *E*) Body weight (*D*) and DAI (*E*) of mice that received regular drinking water plus 50 μL H_2O via enema (H_2O + H_2O, black line), or 3% DSS-containing water plus 50 μL H_2O via enema (DSS + H_2O, blue line), or 3% DSS combined with 25 mg/kg ACh in 50 μL H_2O via enema (DSS + ACh, red line) were monitored and evaluated daily ($n = 6$). (*F*) Representative colon images and colon lengths were measured on day 7 ($n = 6$). (*G*) Representative hematoxylin and eosin (H&E) image of colon sections and corresponding histological scores on day 7 ($n = 6$). (Scale bar, 200 μm.) (*H* and *I*) mRNA (*H*) and protein levels (*I*) of pro- or antiinflammatory cytokines in colon tissues were measured on day 7 by qRT-PCR and ELISA ($n = 5$), respectively. Data are expressed as mean ± SEM and representative results are one of three independent experiments. Statistical differences were tested using unpaired two-tailed Student's *t* test in *B* and *C*, two-way ANOVA in *D* and *E*, and one-way ANOVA in *F*–*I*, followed by post hoc Bonferroni's test. $^*P < 0.05$, $^{**}P < 0.01$, and $^{***}P < 0.001$.

of M-MDSCs under 5-fluorouracil (5-Fu)-induced apoptosis (*SI Appendix*, Fig. S7*B*), which may partially explain the increased frequency of M-MDSCs. In the meantime, expression of C-C motif chemokine receptor 2 (CCR2) on M-MDSCs was enhanced upon ACh stimulation (*SI Appendix*, Fig. S7*C*), indicating recruitment from circulation may also be partly responsible for increased M-MDSCs in vivo.

More importantly, Ly6C expression and IL-10^+ percentage were much higher in ACh-stimulated M-MDSCs than those in nonstimulated M-MDSCs, while nitric oxide synthase 2 (NOS2) and arginase-1 (Arg-1) were unaffected (Fig. 4 *A* and *B* and *SI Appendix*, Fig. S7*D*). The production of IL-10 in the culture supernatant of ACh-stimulated M-MDSCs was also largely increased (Fig. 4*C*). In addition, we obtained M-MDSCs from culturing sorted lineage-negative stem and progenitor cells with GM-CSF and IL-6. Consistently, ACh stimulation tremendously increased the percentage of IL-10^+ M-MDSCs (*SI Appendix*, Fig. S7*E*). In order to evaluate the contribution of ACh-induced IL-10 production to the antiinflammatory effects of M-MDSCs, purified wild-type (IL$10^{+/+}$) and IL-10 knockout (IL$10^{-/-}$)

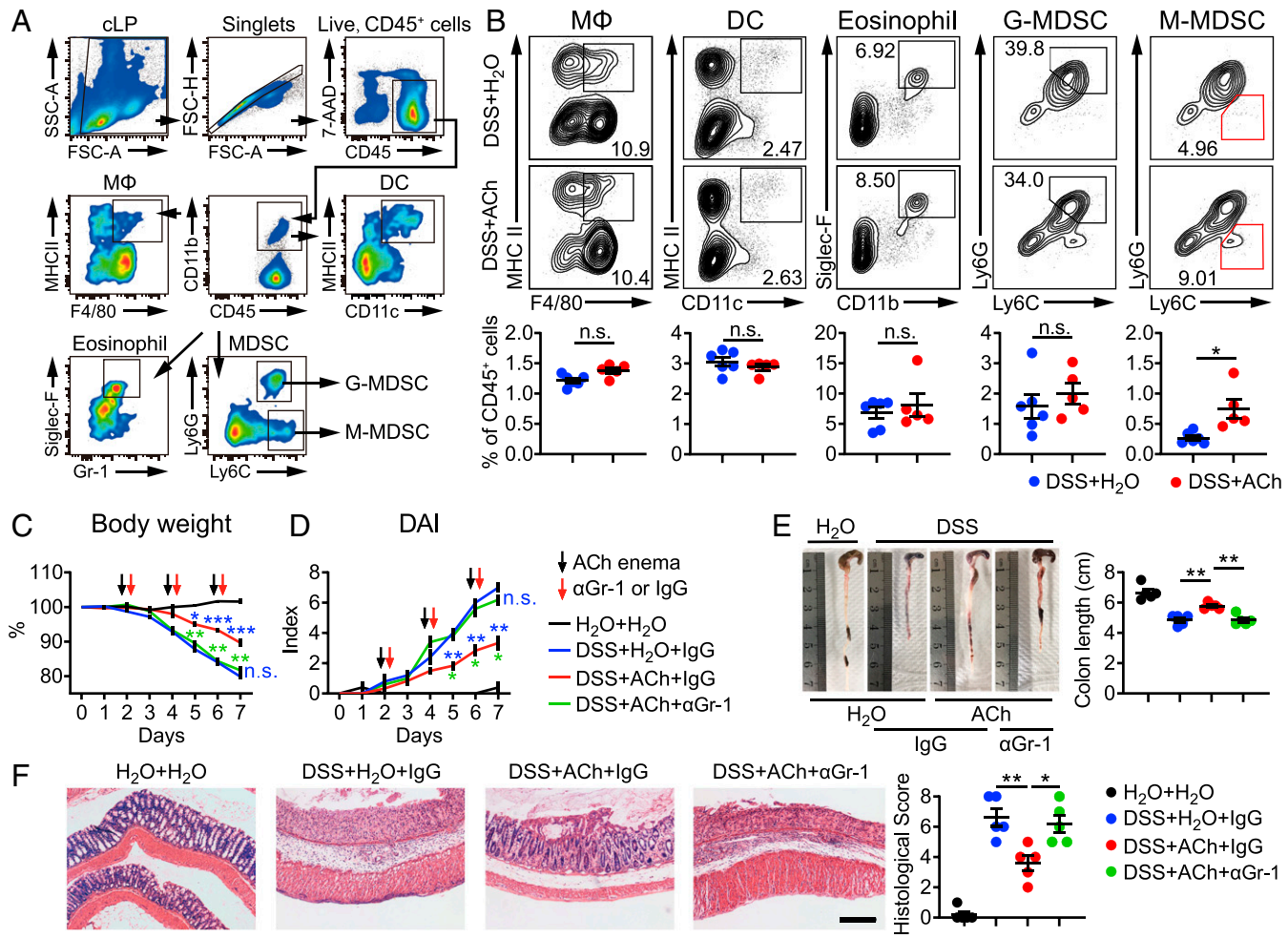

Fig. 3. M-MDSCs are critical for ACh-mediated resistance against colitis. C57BL/6 mice receiving water containing 3% DSS (wt/vol) or regular drinking water alone for 7 d, were treated with 50 μL H_2O (DSS + H_2O) or ACh (25 mg/kg, DSS + ACh) via enema every other day for a total of three times, starting from day 2. (*A* and *B*) On day 7, these mice were killed to determine the subsets of colon-infiltrating myeloid cells (*A* and *B*) and T cells (*B*) by flow cytometry ($n = 6$, DSS + H_2O; $n = 5$, DSS + ACh). (*C* and *D*) For the MDSC depletion experiment, anti-Gr-1 antibody (αGr-1) or isotype control antibody (IgG) was administrated intraperitoneally (10 mg/kg) on days 2, 4, and 6. Body mass (*C*), and DAI (*D*) of control mice treated with H_2O enema (H_2O + H_2O) and colitis mice treated with H_2O enema (DSS + H_2O), ACh enema plus IgG (DSS + ACh + IgG), or ACh enema plus αGr-1 (DSS + ACh + αGr-1) were monitored daily ($n = 5$). For statistical comparisons, blue asterisk (*, **, and ***) indicates DSS + H_2O + IgG vs. DSS + ACh + IgG, green asterisk (* and **) indicates DSS + ACh + αGr-1 vs. DSS + ACh + IgG, n.s. in blue indicates DSS + H_2O + IgG vs. DSS + ACh + αGr-1. (*E*) Representative colon images and colon lengths on day 7 ($n = 5$). (*F*) Representative H&E image of colon sections and corresponding histological scores on day 7 ($n = 5$). (Scale bar, 200 μm.) Data are expressed as mean ± SEM and representative results are one of three independent experiments. Statistical differences were tested using unpaired two-tailed Student's *t* test in *B*, two-way ANOVA in *C* and *D*, and one-way ANOVA in *E* and *F*, followed by post hoc Bonferroni's test. $*P < 0.05$ and $**P < 0.01$, n.s., not significant.

M-MDSCs were prestimulated with or without ACh for 24 h and then cocultured with T cells, respectively. After an additional 16 h, αCD3/αCD28-induced activation and cytokines production of T cells were detected by flow cytometry. Obviously, the expression of activation markers CD69, CD25, and reactive oxygen species (ROS) on T cells was markedly decreased, and the production of IFN-γ and TNF-α in T cells was greatly reduced when cocultured with ACh-stimulated $IL10^{+/+}$ M-MDSCs, compared with those of T cells cocultured with unstimulated $IL10^{+/+}$ M-MDSCs (Fig. 4*D*). But no matter whether in the presence of ACh or not, $IL10^{-/-}$ M-MDSCs lost the inhibition of activation marker expression and cytokine production of T cells (Fig. 4*D*). Moreover, we performed in vivo experiments to further determine the IL-10-dependent inhibitory effect of M-MDSCs on colitis. DSS-induced colitis mice were administrated αGr-1 antibody to deplete M-MDSCs, supplemented with exogenous recombinant murine IL-10 and ACh administration. Remarkably, IL-10 recovered the ACh-mediated benefit on weight loss (Fig. 4*E*), DAI (Fig. 4*F*), colon length shortening (Fig. 4*G*), and pathology (Fig. 4*H*) in absence of M-MDSCs. Therefore, these in vitro and in vivo results demonstrate that ACh enlarges IL-10 production of M-MDSCs to enhance antiinflammatory effects, and hence alleviates intestinal inflammation.

ACh Enlarges IL-10 Production of M-MDSCs via nAChR and the Downstream ERK Pathway. Finally, to uncover the molecular mechanism of ACh effect on promoting IL-10 production of M-MDSCs, M-MDSCs were sorted from cLP of DSS-induced colitis mice and stimulated with or without ACh for RNA-seq. The gene set enrichment analysis identified that neuroactive ligand receptor interaction and the calcium signaling pathway were activated by ACh treatment (*SI Appendix*, Fig. S8*A*). The result of the Kyoto Encyclopedia of Genes and Genomes analysis was also shown (*SI Appendix*, Fig. S8*B*). To further determine which kind of AChR is involved in the effect of ACh on M-MDSCs, we first analyzed the subunits of AChRs expressed

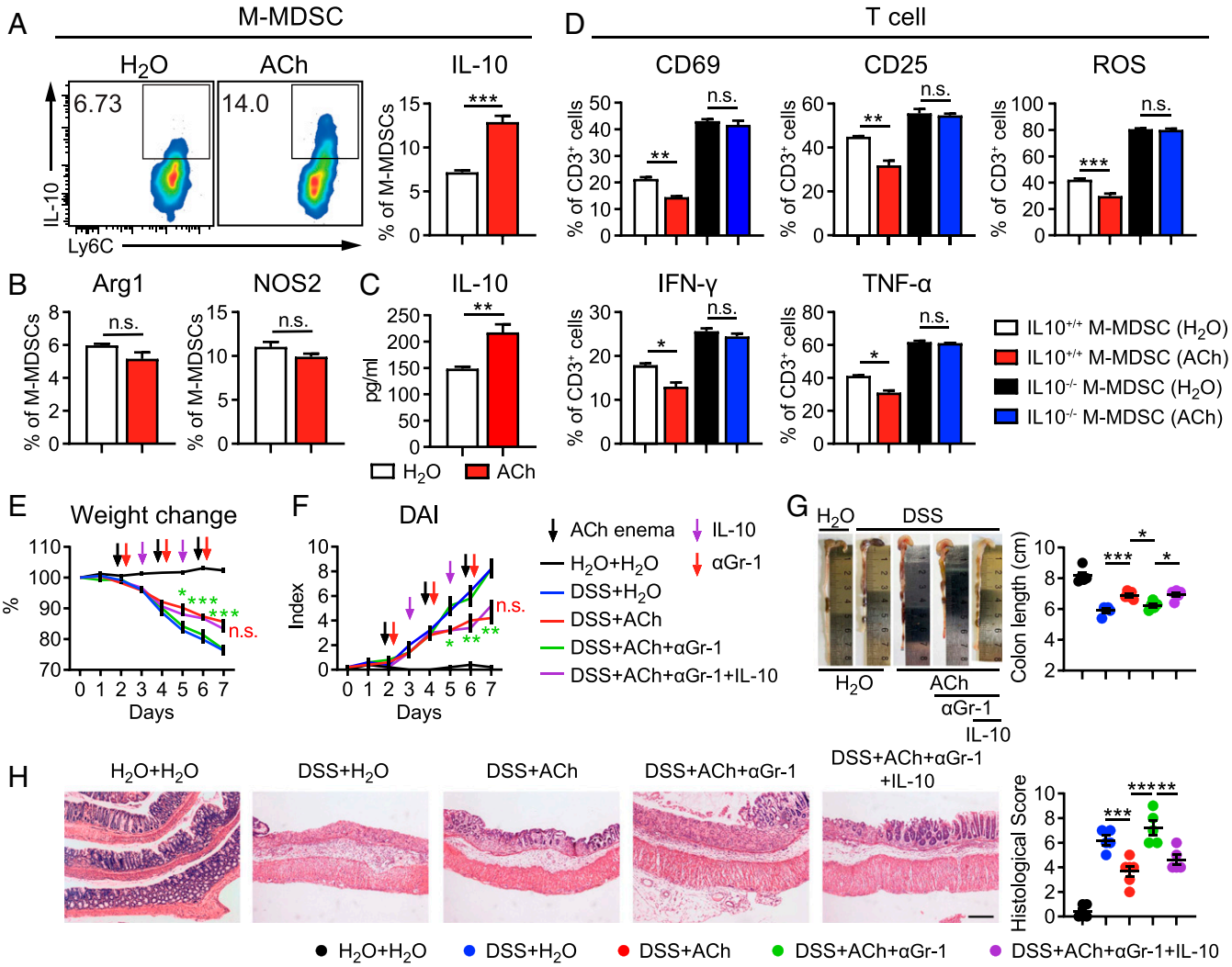

Fig. 4. ACh enhances the antiinflammatory effects of M-MDSCs by enlarging IL-10 production. (*A* and *B*) M-MDSCs purified from DSS-induced colitis mice were stimulated with 100 μM ACh or the equal volume of H_2O for 24 h. The expression of IL-10 (*A*), Arg1, and NOS2 (*B*) on M-MDSCs was determined by flow cytometry ($n = 4$). (*C*) The level of IL-10 in the culture supernatant of M-MDSCs was measured by ELISA ($n = 4$). (*D*) $IL10^{+/+}$ M-MDSCs and $IL10^{-/-}$ M-MDSCs were isolated and prestimulated with H_2O or ACh for 24 h, followed by coculture with T cells at the ratio of 1:4. After additional 16 h, CD25, CD69, ROS, TNF-α, and IFN-γ expressions of T cells were detected by flow cytometry ($n = 3$). (*E*) Female C57BL/6 mice received water containing 3% DSS (wt/vol) or regular drinking water alone for 7 d and were treated with 50 μL H_2O or 25 mg/kg ACh in 50 μL H_2O via enema every other day, starting from day 2 ($n = 5$). αGr-1 or IgG was administrated intraperitoneally (10 mg/kg) on days 2, 4, and 6. Exogenous recombinant mouse IL-10 was administrated intraperitoneally (20 μg/kg, dissolved in 100 μL PBS) at days 3 and 5. (*E* and *F*) Body weight (*E*) and DAI (*F*) of these mice were monitored and evaluated daily ($n = 5$). (*G*) Representative colon images and colon lengths on day 7 ($n = 5$). For statistical comparisons, red asterisk (*) indicates DSS + ACh+ IgG vs. DSS + ACh + αGr-1, green asterisk (*) indicates DSS + ACh + αGr-1 vs. DSS + ACh + αGr-1 + IL-10, and n.s. in red indicates DSS + ACh vs. DSS + ACh + αGr-1 + IL-10. (*H*) Representative H&E image of distal colon sections and corresponding histological scores on day 7 ($n = 5$). (Scale bar, 200 μm.) Data are expressed as mean ± SEM and representative results are one of three independent experiments. Statistical differences were tested using unpaired Student's *t* test (two-tailed) in *A*–*C*, one-way ANOVA in *D*, *G*, and *H*, and two-way ANOVA in *E* and *F*, followed by post hoc Bonferroni's test. $*P < 0.05$, $**P < 0.01$, and $***P < 0.001$, n.s., not significant.

on M-MDSCs according to RNA-seq data. Strong or moderate expression levels of nAChR subunit genes, including Chrne, Chrna2, Chrnb1, and Chrnb2 were detected on colonic M-MDSCs, while only weak expression of mAChR subunit gene Chrm3 was tested (Fig. 5*A*). Furthermore, atropine (Atrop) and mecamylamine (Mecam) were used to block mAChR and nAChR on M-MDSCs, respectively. Strikingly, treatment of mecamylamine totally reversed ACh-induced increased frequency of $IL\text{-}10^+$ M-MDSCs, while atropine showed no effect, compared with the control group (Fig. 5*B*). In the meantime, we found that the up-regulated production of IL-10 in the culture supernatant of ACh-treated M-MDSCs was reverted by treatment of mecamylamine but not atropine (Fig. 5*C*). Thus, these results strongly suggest that ACh enlarges IL-10 production of M-MDSCs via nAChR.

According to RNA-seq data and the protein–protein interaction network analysis, there were 21 representative MAPK/ERK pathway-related genes significantly up-regulated in response to ACh stimulation, including RAS (Hras, Nras), Mek (Map2k1), and Erk (Mapk1) (Fig. 5 *D* and *E*). Therefore, purified M-MDSCs were stimulated with ACh and the level of pERK was analyzed at the indicated times. The mean fluorescence intensity (MFI) of pERK in M-MDSCs was significantly increased at 30 min, 60 min, and 240 min post-ACh stimulation (Fig. 5*F*). Furthermore, when the phosphorylation of ERK in M-MDSCs was abrogated by trametinib, SCH772984, or U0126, ACh lost its ability to promote IL-10 production in M-MDSCs (Fig. 5*G*),

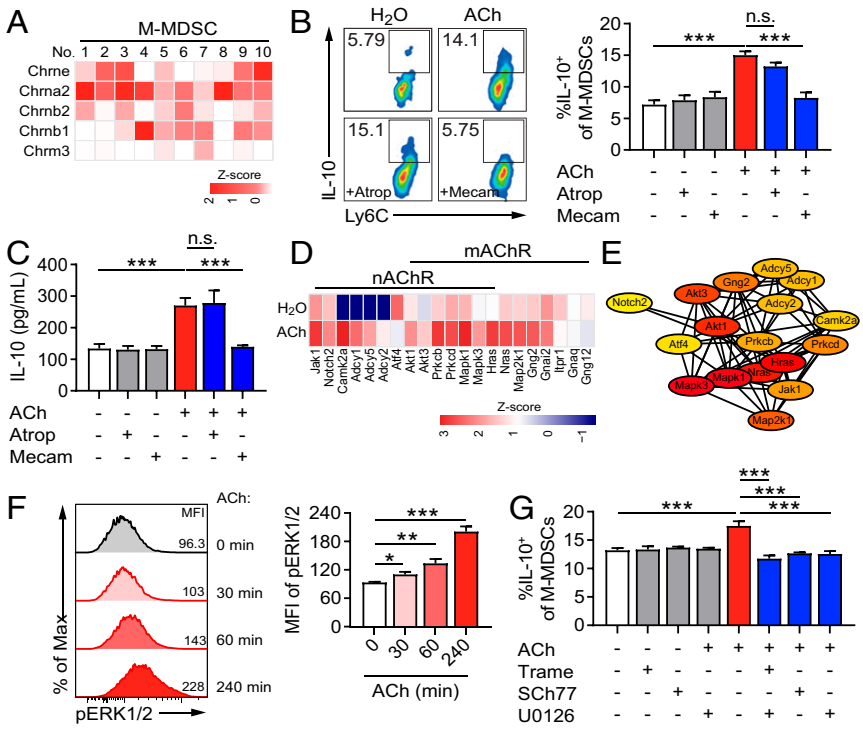

Fig. 5. ACh up-regulates IL-10 release of M-MDSCs through activating the nAChR/ERK pathway. (*A*, *D*, and *E*) M-MDSCs isolated from the cLP of DSS-induced mice were stimulated with 100 μM ACh or the equal volume of H_2O for 16 h and collected for RNA-seq. (*B, C, F*, and *G*) M-MDSCs were generated by culturing sorted lineage-negative stem and progenitor cells with GM-CSF and IL-6 for 4 d. (*A*) The heatmap was used to display the expression profile of AChR subunits on M-MDSCs (n = 10). (*B* and *C*) Generated M-MDSCs were pretreated with or without nAChR antagonist mecamylamine (Mecam, 10 μM) or mAChR antagonist atropine (Atrop, 10 μM) for 30 min and then stimulated with or without 100 μM ACh. After additional 24 h, (*B*) the proportion of IL-10$^+$ M-MDSCs was determined by flow cytometry (n = 4), and (*C*) IL-10 production in the culture supernatants of M-MDSCs was determined by ELISA (n = 4). (*D*) The downstream genes of nAChR and mAChR activated by ACh treatment (n = 4). (*E*) The protein–protein interaction network of target genes from ACh-stimulated M-MDSCs. The ellipse nodes represent target and the colors of nodes from red to yellow represent the descending order of degree values. Genes with degree values <2 were excluded. (*F*) M-MDSCs were stimulated with ACh (100 μM) and the MFI of pERK1/2 was determined at indicated times by flow cytometry. (*G*) M-MDSCs were pretreated with or without MEK/ERK inhibitors trametinib (10 μM), SCH772984 (10 μM), or U0126 (10 μM) for 30 min, and then stimulated with or without 100 μM ACh. After an additional 24 h, the proportion of IL-10$^+$ M-MDSCs was determined by flow cytometry (n = 3). Data are expressed as mean ± SEM and representative results are one of three independent experiments. All statistical differences were tested using one-way ANOVA followed by post hoc Bonferroni's test. *P < 0.05, **P < 0.01, and ***P < 0.001, n.s., not significant.

indicating that the ACh-induced IL-10$^+$ M-MDSC increase depended on the ERK-involved pathway.

Discussion

ACh is mainly synthesized by cholinergic neurons that constitute the ENS (5, 12). As one of the major neurotransmitters, ACh has been found to take part in the regulation of inflammation in the peripheral nervous system (6, 12). However, it remains unclear whether and how the immune regulation of ACh is involved in the pathogenesis of IBD. In this study, we first observed severe disruption of neuronal architecture and impaired ACh production in the ENS during IBDs. Furthermore, an ACh enema could ameliorate colitis by enhancing the IL-10 production of M-MDSCs through activating the nAChR/ERK pathway. Thus, our results uncover an ACh-mediated neuroimmunoregulatory pathway in IBDs, which contributes to mitigating intestinal inflammation and provides a potential therapeutic strategy for IBDs.

The ENS is represented as a complicated neuronal network and is widely located in the intestinal wall (2). How the ENS is altered in IBDs remained inconclusive for a long time before the emergence and utilization of whole-field optical technology. Many previous studies even yielded conflicting conclusions regarding the alteration of the ENS (8, 11, 36). Until 2016, iDISCO was used to reveal the bacteria-infected intestinal tissue and 3D view of ENS architecture, which provided insights into the spatial localization between neuronal networks and the immune system (37). In this study, we applied iDISCO-based whole-mount immunostaining to display the neuronal network of the ENS in both IBD patients and colitis mice and clearly exhibited the loss of neurons and the destruction of the neuronal network structure. Meanwhile, by using xCell, a robust method that converts gene expression profiles to enrichment scores of cell types across samples, we verified the shrinkage in percentage of neurons in the colon of IBD patients. Therefore, our findings demonstrate the impairment of the ENS during IBD by applying a 3D imaging of the whole-mount approach instead of two-dimensional (2D) sections routinely used, which is further evidenced by computational cellular composition estimation.

More importantly, involvement of the impaired ENS in IBDs requires further investigation. It has been well known that the communication between the ENS and immune system can modulate the inflammatory response via the release of neurotransmitters (5, 6, 12). As previously mentioned, ACh is thought to be the most important neurotransmitter in the ENS. Evidence that the ACh-related cholinergic pathway could remarkably impact the pathogenesis of IBDs comes from the effect of smoking in UC patients (38, 39). In addition, administration of α7 nAChR agonists or acetylcholinesterase inhibitors, including clinically approved galantamine, results in mitigation of colitis in mice (40–43). Their antiinflammatory effects are mainly attributed to the vagus nerve-based splenic pathway, in which situation these cholinergic reagents need be administrated systemically. But in

this study, we observed the dysfunction of the cholinergic pathway in the ENS, and further demonstrated that local infusion of ACh, which was confirmed reduced in colitis, could ameliorate intestinal inflammation in mice via modulating M-MDSCs in the cLP. In this regard, strategies to restore the damaged ENS or to activate the locally colonic ACh-related cholinergic pathway are expected to provide benefit to IBD patients.

Both nAChRs and mAChRs have been demonstrated to express on various immune cells including T cells, B cells, and macrophages (44, 45). Thus, the interaction between ACh and immune cells may serve as the underlying mechanism of the above findings. M-MDSCs, as one subset of MDSCs, have mononuclear morphology, and express a variety of surface-bound and secreted factors such as IL-10 to suppress T-cell-mediated immunity on colitis (16, 19, 20, 27). In addition, M-MDSCs possess more potent inhibitory activity than the other subset of MDSCs, G-MDSCs (18, 23). Although the antiinflammatory role of MDSCs has been widely studied, it is often ignored to distinguish M-MDSCs from G-MDSCs, and research on neuroimmune regulation of MDSCs during colitis is not fully investigated before. In the present study, we provided evidence for the expression of mAChRs and nAChRs on M-MDSCs and identified M-MDSCs but not G-MDSCs as the most important target immune cells that were directly modulated by ACh. It is noteworthy that AChR activation allows the influx of $Ca2^{+}$, which stimulates the downstream signaling pathways including the ERK pathway (46, 47). The increased ERK activation has been reported responsible for enlarging IL-10 production in macrophages, T cells, and B cells (48, 49). As anticipated, ACh treatment promoted IL-10 secretion of M-MDSCs via ERK activation. Hence, a nAChR/ERK/IL-10 axis in M-MDSCs was identified in this study. Moreover, besides the alteration of increased M-MDSCs, the decreased Th17 cells were observed in the cLP of colitis mice after an ACh enema, but ACh didn't directly impact Th17 proliferation and differentiation. Accordingly, we speculate the elevated infiltration and enhanced anti-inflammatory effects of M-MDSCs might contribute to the declined Th17 population, which is in agreement with a previous study showing significantly lower Th17 cell levels in MDSC recipient mice (43).

In conclusion, we have demonstrated the disrupted ENS and reduced colonic ACh release in both IBD patients and colitis mice. In addition, ACh was found to directly participate in the pathogenesis of IBDs via reinforcing the antiinflammatory effects of M-MDSCs. Together, these findings highlight the role of ACh-mediated neuroimmunoregulation and may provide further support for therapeutic approaches to IBDs.

Materials and Methods

For more details, please refer to *SI Appendix, Supplemental Materials and Methods*.

Microarray Data Processing and xCell Analysis. The gene expression profiling datasets (GSE38713) were obtained from the GEO database (https://www.ncbi.nlm.nih.gov/geo/). A total of 43 samples were measured in this array. Estimation of neuron fractions from colon tissues of UC patients was determined through gene expression analysis (GSE38713) using xCell (https://xcell.ucsf.edu/) (29). Pearson's correlation coefficient between gene expression and percentage of neurons was calculated and visualized using R software.

Animals. Female C57BL/6 mice (age 6 to 8 wk) were obtained from Shanghai Super-B&K Laboratory Animal Co., Ltd. and Shanghai SLAC Laboratory Animal Co., Ltd. IL-$10^{-/-}$ mice (B6.129P2-Il10^{tm1cgn}/J) with the C57BL/6 background were purchased from The Jackson Laboratory. These mice were specific pathogen-free and bred and housed at the Animal Care Facility of Fudan University under laboratory conditions (23 °C, 50% humidity, 12/12 h light/dark). The experimental protocol was approved by the Institutional Animal Care and Use Committee of Fudan University (2018JS-056) following the Guidelines for the Care and Use of Laboratory Animals (No. 55 issued by the Ministry of Health, China on January 25th, 1998).

Human Samples. Colon mucosa samples were collected from UC patients and healthy subjects from the sigmoid colon during endoscopy at the Department of Digestive Diseases, Huashan Hospital of Fudan University, Shanghai, China. Informed consent was obtained from all subjects involved and the project was approved by the Ethical Committee of Medical Research, Huashan Hospital of Fudan University (No. 2013–005).

iDISCO and Whole-Mount Immunostaining. iDISCO-based tissue clearing for whole-mount immunostaining of colons from DSS-induced colitis mice and humans was performed according to a previous protocol (30). Briefly, murine colon tissues were precut longitudinally and cleaned with prechilled phosphate buffered saline (PBS). Samples were fixed in 4% paraformaldehyde (PFA), then dehydrated with gradual addition of methanol in PBS (20 to 80%). Bleaching with 5% H_2O_2 in methanol was done at 4 °C overnight, then rehydrated and permeabilized with 0.2% Triton X-100.

After that, samples were incubated overnight with 0.16% Triton X-100/20% dimethylsulfoxide (DMSO)/0.3 M glycine in PBS at 37 °C followed by 0.17% Triton X-100/10% DMSO/3% donkey serum in PBS for 8 h. After blocking, the samples were washed for 1 h twice in PBS with 0.2% Tween-20 and 10 mg/mL heparin (PTwH), and then incubated with mouse anti-NF-M/H antibody (Biolegend, 1: 200) in primary antibody dilutions (PTwH/5% DMSO/3% donkey serum) at 37 °C for 48 h. For dual immunostaining, samples were incubated with mouse anti-NF-M/H antibody and goat anti-ChAT antibody (Sigma-Aldrich, 1: 200). Next, samples were washed with PTwH for 1 d and incubated with donkey anti-mouse IgG H&L (Alexa Fluor 647; Abcam) in 0.2% PTwH/5% DMSO/3% donkey serum (1: 400) at 37 °C. Or samples were incubated with donkey anti-mouse and donkey anti-goat IgG H&L (Alexa Fluor 647, Alexa Fluor 405; Abcam) secondary antibodies (1:400). After 48 h, samples were extensively washed with PTwH for 2 d with periodic solution change. For sample clearing, samples were subjected to successive washes in 66% dichloromethane (DCM)/33% methanol, 100% DCM, and 100% dibenzyl ether (Sigma-Aldrich).

Last, samples were imaged using a multiphoton laser scanning microscope and a 25×/1.05 NA objective lens (FVMPE-RS, Olympus). An infrared laser of 1,100 nm was used as excitation wavelength. For dual-label immunohistochemistry, images were acquired using an Olympus FV3000 confocal microscope (Olympus). Images were analyzed using cellSens (Olympus) and ImageJ.

Induction of Colitis and Treatment. Intestinal inflammation was induced by adding 3% DSS into drinking water for 7 d. For the experiment to determine the effect of ACh on colitis, mice were treated with 50 μL H_2O or ACh (25 mg/kg, dissolved in H_2O) via enema every other day, starting from day 2 for a total of three times. For the MDSC depletion experiment, αGr-1 antibody (RB6-8C5; BioXCell) or isotype control IgG (Rat IgG2b; BioXCell) was administrated intraperitoneally (i.p.; 10 mg/kg) every other day, starting from day 2 for a total of three times. IL-10 was injected i.p. at a dose of 20 μg/kg, and the ACh enema was performed the same as above. DAI was used to describe severity of colitis by combining the scores of bleeding, stool, and weight loss according to previous studies (31, 33).

MDSC Generation In Vitro. Bone marrow of C57BL/6 mice was collected and followed by isolation of lineage-negative stem and progenitor cells using a mouse direct lineage cell depletion kit (Miltenyi Biotec) according to the manufacturer's instruction. To differentiate lineage-negative cells into MDSCs, lineage-negative cells were placed in each well of 24-well plates and cultured in RPMI 1640 (10% fetal bovine serum (FBS), 5% sodium pyruvate, 1% penicillin/steptomycin, and 10 mM Hepes) containing granulocyte-macrophage colony stimulating factor (GM-CSF; 40 ng/mL; PeproTech) and IL-6 (10 ng/mL; PeproTech) for 4 d. Then, cells were treated with or without ACh and collected at indicated times for analysis.

Statistical Analysis. Data were expressed as mean ± SEM and analyzed by two-tailed Student's *t* test, one-way analysis of variance, and two-way analysis of variance followed by Bonferroni posttest. Statistical analysis was performed with GraphPad Prism 8.0 software (GraphPad Software). Results were considered significant when P value was <0.05.

Data Availability. All study data are included in the article and/or supporting information.

ACKNOWLEDGMENTS. This work was supported by the National Natural Science Foundation of China (81870375, 81600438, and 81630016), the Shanghai Rising-Star Program (18QA1401000). We thank Mrs. Jing Qian of Fudan University for excellent technical assistance.

1. J. B. Furness, The enteric nervous system and neurogastroenterology. *Nat. Rev. Gastroenterol. Hepatol.* **9**, 286–294 (2012).
2. M. Rao, M. D. Gershon, Neurogastroenterology: The dynamic cycle of life in the enteric nervous system. *Nat. Rev. Gastroenterol. Hepatol.* **14**, 453–454 (2017).
3. J. B. Furness, L. R. Rivera, H. J. Cho, D. M. Bravo, B. Callaghan, The gut as a sensory organ. *Nat. Rev. Gastroenterol. Hepatol.* **10**, 729–740 (2013).
4. F. De Vadder *et al*., Gut microbiota regulates maturation of the adult enteric nervous system via enteric serotonin networks. *Proc. Natl. Acad. Sci. U.S.A.* **115**, 6458–6463 (2018).
5. K. G. Margolis, M. D. Gershon, Enteric neuronal regulation of intestinal inflammation. *Trends Neurosci.* **39**, 614–624 (2016).
6. L. M. Costes, G. E. Boeckxstaens, W. J. de Jonge, C. Cailotto, Neural networks in intestinal immunoregulation. *Organogenesis* **9**, 216–223 (2013).
7. D. R. Plichta, D. B. Graham, S. Subramanian, R. J. Xavier, Therapeutic opportunities in inflammatory bowel disease: Mechanistic dissection of host-microbiome relationships. *Cell* **178**, 1041–1056 (2019).
8. N. Bernardini *et al*., Immunohistochemical analysis of myenteric ganglia and interstitial cells of Cajal in ulcerative colitis. *J. Cell. Mol. Med.* **16**, 318–327 (2012).
9. P. Brun *et al*., Toll-like receptor 2 regulates intestinal inflammation by controlling integrity of the enteric nervous system. *Gastroenterology* **145**, 1323–1333 (2013).
10. K. Nurgali *et al*., Morphological and functional changes in Guinea-pig neurons projecting to the ileal mucosa at early stages after inflammatory damage. *J. Physiol.* **589**, 325–339 (2011).
11. K. G. Margolis *et al*. Enteric neuronal density contributes to the severity of intestinal inflammation. *Gastroenterology* **141**, 588–598, 598.e1–582 (2011).
12. B. B. Yoo, S. K. Mazmanian, The enteric network: Interactions between the immune and nervous systems of the gut. *Immunity* **46**, 910–926 (2017).
13. H. Wang *et al*., Nicotinic acetylcholine receptor alpha7 subunit is an essential regulator of inflammation. *Nature* **421**, 384–388 (2003).
14. Y. X. Fujii *et al*., Diminished antigen-specific IgG1 and interleukin-6 production and acetylcholinesterase expression in combined M1 and M5 muscarinic acetylcholine receptor knockout mice. *J. Neuroimmunol.* **188**, 80–85 (2007).
15. S. Budhwar, P. Verma, R. Verma, S. Rai, K. Singh, The yin and yang of myeloid derived suppressor cells. *Front. Immunol.* **9**, 2776 (2018).
16. D. I. Gabrilovich, S. Nagaraj, Myeloid-derived suppressor cells as regulators of the immune system. *Nat. Rev. Immunol.* **9**, 162–174 (2009).
17. K. Ohl, K. Tenbrock, Reactive oxygen species as regulators of MDSC-mediated immune suppression. *Front. Immunol.* **9**, 2499 (2018).
18. Y. Zhao, T. Wu, S. Shao, B. Shi, Y. Zhao, Phenotype, development, and biological function of myeloid-derived suppressor cells. *OncoImmunology* **5**, e1004983 (2015).
19. B. Knier *et al*., Myeloid-derived suppressor cells control B cell accumulation in the central nervous system during autoimmunity. *Nat. Immunol.* **19**, 1341–1351 (2018).
20. C. R. Lee *et al*., Myeloid-derived suppressor cells are controlled by regulatory T cells via TGF-β during murine colitis. *Cell Rep.* **17**, 3219–3232 (2016).
21. D. V. Ostanin, D. Bhattacharya, Myeloid-derived suppressor cells in the inflammatory bowel diseases. *Inflamm. Bowel Dis.* **19**, 2468–2477 (2013).
22. M. L. Ibrahim *et al*., Myeloid-derived suppressor cells produce IL-10 to elicit DNMT3b-dependent IRF8 silencing to promote colitis-associated colon tumorigenesis. *Cell Rep.* **25**, 3036–3046.e6 (2018).
23. V. Bronte *et al*., Recommendations for myeloid-derived suppressor cell nomenclature and characterization standards. *Nat. Commun.* **7**, 12150 (2016).
24. U. P. Singh *et al*., Role of resveratrol-induced CD11b(+) Gr-1(+) myeloid derived suppressor cells (MDSCs) in the reduction of CXCR3(+) T cells and amelioration of chronic colitis in IL-10(-/-) mice. *Brain Behav. Immun.* **26**, 72–82 (2012).
25. L. A. Haile *et al*. Myeloid-derived suppressor cells in inflammatory bowel disease: A new immunoregulatory pathway. *Gastroenterology* **135**, 871–881, 881.e1–875 (2008).
26. E. Kontaki *et al*., Aberrant function of myeloid-derived suppressor cells (MDSCs) in experimental colitis and in inflammatory bowel disease (IBD) immune responses. *Autoimmunity* **50**, 170–181 (2017).
27. Q. Guan *et al*., The role and potential therapeutic application of myeloid-derived suppressor cells in TNBS-induced colitis. *J. Leukoc. Biol.* **94**, 803–811 (2013).
28. Y. Liu *et al*., Lactoferrin-induced myeloid-derived suppressor cell therapy attenuates pathologic inflammatory conditions in newborn mice. *J. Clin. Invest.* **129**, 4261–4275 (2019).
29. D. Aran, Z. Hu, A. J. Butte, xCell: Digitally portraying the tissue cellular heterogeneity landscape. *Genome Biol.* **18**, 220 (2017).
30. N. Renier *et al*., iDISCO: a simple, rapid method to immunolabel large tissue samples for volume imaging. *Cell* **159**, 896–910 (2014).
31. S. Wirtz *et al*., Chemically induced mouse models of acute and chronic intestinal inflammation. *Nat. Protoc.* **12**, 1295–1309 (2017).
32. H. S. de Souza, C. Fiocchi, Immunopathogenesis of IBD: Current state of the art. *Nat. Rev. Gastroenterol. Hepatol.* **13**, 13–27 (2016).
33. J. C. Masterson *et al*., Eosinophil-mediated signalling attenuates inflammatory responses in experimental colitis. *Gut* **64**, 1236–1247 (2015).
34. P. Giuffrida, A. Di Sabatino, Targeting T cells in inflammatory bowel disease. *Pharmacol. Res.* **159**, 105040 (2020).
35. S. N. Harbour, C. L. Maynard, C. L. Zindl, T. R. Schoeb, C. T. Weaver, Th17 cells give rise to Th1 cells that are required for the pathogenesis of colitis. *Proc. Natl. Acad. Sci. U.S.A.* **112**, 7061–7066 (2015).
36. Y. Obata, V. Pachnis, The effect of microbiota and the immune system on the development and organization of the enteric nervous system. *Gastroenterology* **151**, 836–844 (2016).
37. I. Gabanyi *et al*., Neuro-immune interactions drive tissue programming in intestinal macrophages. *Cell* **164**, 378–391 (2016).
38. M. G. Frank, H. Srere, C. Ledezma, B. O'Hara, H. C. Heller, Prenatal nicotine alters vigilance states and AchR gene expression in the neonatal rat: Implications for SIDS. *Am. J. Physiol. Regul. Integr. Comp. Physiol.* **280**, R1134–R1140 (2001).
39. C. M. Hernandez, A. V. Terry Jr, Repeated nicotine exposure in rats: Effects on memory function, cholinergic markers and nerve growth factor. *Neuroscience* **130**, 997–1012 (2005).
40. A. Grandi *et al*., α_7 nicotinic agonist AR-R17779 protects mice against 2,4,6-trinitrobenzene sulfonic acid-induced colitis in a spleen-dependent way. *Front. Pharmacol.* **8**, 809 (2017).
41. S. P. Singh *et al*., Acetylcholinesterase inhibitor pyridostigmine bromide attenuates gut pathology and bacterial dysbiosis in a murine model of ulcerative colitis. *Dig. Dis. Sci.* **65**, 141–149 (2020).
42. S. A. Wazea, W. Wadie, A. K. Bahgat, H. S. El-Abhar, Galantamine anti-colitic effect: Role of alpha-7 nicotinic acetylcholine receptor in modulating Jak/STAT3, NF-κB/HMGB1/RAGE and p-AKT/Bcl-2 pathways. *Sci. Rep.* **8**, 5110 (2018).
43. H. Ji *et al*., Central cholinergic activation of a vagus nerve-to-spleen circuit alleviates experimental colitis. *Mucosal Immunol.* **7**, 335–347 (2014).
44. T. Fujii *et al*., Expression and function of the cholinergic system in immune cells. *Front. Immunol.* **8**, 1085 (2017).
45. K. Kawashima, K. Yoshikawa, Y. X. Fujii, Y. Moriwaki, H. Misawa, Expression and function of genes encoding cholinergic components in murine immune cells. *Life Sci.* **80**, 2314–2319 (2007).
46. D. L. Li *et al*., Acetylcholine inhibits hypoxia-induced tumor necrosis factor-α production via regulation of MAPKs phosphorylation in cardiomyocytes. *J. Cell. Physiol.* **226**, 1052–1059 (2011).
47. B. K. Kim *et al*., IL-6 attenuates trimethyltin-induced cognitive dysfunction via activation of JAK2/STAT3, M1 mAChR and ERK signaling network. *Cell. Signal.* **25**, 1348–1360 (2013).
48. S. Garaud *et al*., CD5 expression promotes IL-10 production through activation of the MAPK/Erk pathway and upregulation of TRPC1 channels in B lymphocytes. *Cell. Mol. Immunol.* **15**, 158–170 (2018).
49. J. Liu *et al*., TLR2 stimulation strengthens intrahepatic myeloid-derived cell-mediated T cell tolerance through inducing kupffer cell expansion and IL-10 production. *J. Immunol.* **200**, 2341–2351 (2018).